Chemical Science

ROYAL SOCIETY OF CHEMISTRY

EDGE ARTICLE

View Article Online
View Journal | View Issue

Cite this: *Chem. Sci.*, 2022, **13**, 2391

All publication charges for this article have been paid for by the Royal Society of Chemistry

Ligand and solvent effects on CO_2 insertion into group 10 metal alkyl bonds†

Anthony P. Deziel,[a] Matthew R. Espinosa,[a] Ljiljana Pavlovic,[b] David J. Charboneau,[a] Nilay Hazari,*[a] Kathrin H. Hopmann*[b] and Brandon Q. Mercado[a]

The insertion of carbon dioxide into metal element σ-bonds is an important elementary step in many catalytic reactions for carbon dioxide valorization. Here, the insertion of carbon dioxide into a family of group 10 alkyl complexes of the type (^{R}PBP)M(CH_3) (^{R}PBP = $B(NCH_2PR_2)_2C_6H_4^-$; R = Cy or ^{t}Bu; M = Ni or Pd) to generate κ^1-acetate complexes of the form (^{R}PBP)M{$OC(O)CH_3$} is investigated. This involved the preparation and characterization of a number of new complexes supported by the unusual ^{R}PBP ligand, which features a central boryl donor that exerts a strong *trans*-influence, and the identification of a new decomposition pathway that results in C–B bond formation. In contrast to other group 10 methyl complexes supported by pincer ligands, carbon dioxide insertion into (^{R}PBP)M(CH_3) is facile and occurs at room temperature because of the high *trans*-influence of the boryl donor. Given the mild conditions for carbon dioxide insertion, we perform a rare kinetic study on carbon dioxide insertion into a late-transition metal alkyl species using ($^{t^{Bu}}$PBP)Pd(CH_3). These studies demonstrate that the Dimroth–Reichardt parameter for a solvent correlates with the rate of carbon dioxide insertion and that Lewis acids do not promote insertion. DFT calculations indicate that insertion into ($^{t^{Bu}}$PBP)M(CH_3) (M = Ni or Pd) proceeds *via* an S_E2 mechanism and we compare the reaction pathway for carbon dioxide insertion into group 10 methyl complexes with insertion into group 10 hydrides. Overall, this work provides fundamental insight that will be valuable for the development of improved and new catalysts for carbon dioxide utilization.

Received 16th November 2021
Accepted 31st January 2022

DOI: 10.1039/d1sc06346d

rsc.li/chemical-science

Introduction

Carbon dioxide (CO_2) is an attractive target as a chemical feedstock due to its low cost, non-toxic nature, and abundance.[1] Although there are several chemicals currently industrially prepared from CO_2, such as urea and carbonates,[2] only a small fraction of our available CO_2 is used as a source of carbon for either commodity[1h] or fine[3] chemical synthesis. The full exploitation of CO_2 as a feedstock is limited by its kinetic and thermodynamic stability, which poses a scientific challenge for developing synthetic routes to make more valuable chemicals from CO_2. Utilizing homogeneous transition metal catalysts is one attractive approach for solving kinetic problems associated with the conversion of CO_2 into more valuable chemicals and a variety of systems have been developed for the thermal, electrochemical, and photochemical conversion of CO_2.[1,3] An elementary step which is proposed in many of these catalytic reactions is CO_2 insertion into an M–E σ-bond (for example E = H, OR, NR_2, or CR_3) to form a product with a M–O bond (eqn (1)).[4] To date, the majority of catalysts feature late transition metals,[1,3] likely due to the relative weakness of the M–O bonds that are formed,[4] which makes cleavage of the M–O bond and subsequent transformation more facile.

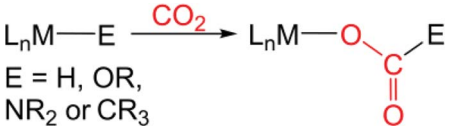

(1)

The crucial role of CO_2 insertion into late transition metal element σ-bonds in catalysis means that understanding the pathway for insertion is important for rationally designing improved catalytic systems.[4] In particular, understanding the impact of the ancillary ligand, solvent, and additives that are commonly used in catalysis, such as Lewis acids, is valuable for the development of optimized catalysts and reaction conditions. Although the influence of these factors on CO_2 insertion into metal hydrides has been studied,[5] there is limited information on how these variables affect CO_2 insertion into metal alkyl bonds.[6–13] These reactions are particularly important because they can result in the generation of products

[a]*Department of Chemistry, Yale University, P. O. Box 208107, New Haven, Connecticut, 06520, USA. E-mail: nilay.hazari@yale.edu*

[b]*Department of Chemistry, UiT The Arctic University of Norway, N-9307 Tromsø, Norway. E-mail: kathrin.hopmann@uit.no*

† Electronic supplementary information (ESI) available. CCDC 2107492–2107496 and 2108774. For ESI and crystallographic data in CIF or other electronic format see DOI: 10.1039/d1sc06346d

containing C–C bonds from CO_2, which has been identified as a high priority research target by the United States National Academies of Science.[2] For example, group 10 catalysts have been used for the reductive carboxylation of a variety of alkyl halides and pseudo halides.[3h,i] In these reactions, C–C bonds are proposed to form between CO_2 and the alkyl electrophile *via* the insertion of CO_2 into a metal alkyl bond.

A major limitation in studying CO_2 insertion into group 10 metal alkyl bonds is the paucity of systems that are stable and react under mild conditions.[14] In fact, the majority of well-defined examples of CO_2 insertion reactions into group 10 metal alkyls require elevated temperatures, long reaction times, and do not give quantitative yields of products, which makes it difficult to perform kinetic studies (Fig. 1a). Due to the need for high temperatures, there has been a focus on complexes supported by pincer ligands, which often result in complexes with high thermal stability. For example, Wendt and co-workers demonstrated that treatment of ($^{t\mathrm{Bu}}$PCP)Pd(CH_3) ($^{t\mathrm{Bu}}$PCP = 2,6-$C_6H_3(CH_2P^tBu_2)_2$) with 4 atm of CO_2 at 80 °C results in complete conversion to the κ^1-acetate complex ($^{t\mathrm{Bu}}$PCP)Pd{OC(O)CH_3}, but the reaction takes two days.[15] Similarly, we reported that the reaction of 1 atm of CO_2 with the related compound ($^{t\mathrm{Bu}}$PCP)Ni(CH_3) requires heating to 150 °C to form the acetate complex ($^{t\mathrm{Bu}}$PCP)Ni{OC(O)CH_3}, but only approximately 75% of the acetate product is formed.[16] Changing the pincer ligand from $^{t\mathrm{Bu}}$PCP to a system containing an sp^3-hybridized carbon donor or replacing one of the phosphine arms of the pincer ligand with a hemi-labile nitrogen donor only leads to small changes in the rate of reaction.[17] A notable example of a group 10 methyl complex that does not contain a pincer ligand and inserts CO_2 at room temperature is an unusual anionic palladium dimethyl complex, with a pendant Lewis acid, prepared by Jordan and co-workers.[7] Although this system inserts CO_2 rapidly it requires careful handling as it is unstable at room temperature. Overall, in order to gain detailed information on the factors that influence the rate of CO_2 insertion there is a need for stable alkyl complexes that cleanly react with CO_2 under mild conditions.

In this work, we describe the insertion of CO_2 into palladium and nickel methyl complexes supported by $^{\mathrm{R}}$PBP ($^{\mathrm{R}}$PBP = $B(NCH_2PR_2)_2C_6H_4^-$; R = Cy or ^{t}Bu) pincer ligands, which contain a strongly donating central boryl donor (Fig. 1b). As a result of the strong *trans*-influence of the boryl donor, these complexes insert CO_2 at significantly milder conditions (room temperature) than previously reported pincer systems. This enables us to measure the kinetics of CO_2 insertion and study the effect of modulating the pincer ligand and the solvent on CO_2 insertion. We demonstrate that the Dimroth–Reichardt $E_T(30)$ parameter[18] for a solvent correlates with the rate of CO_2 insertion and show that Lewis acids, which are often present in catalysis, do not promote CO_2 insertion. Our experimental studies are complemented by computational investigations to understand the pathway for CO_2 insertion and identify the structure of key transition states and intermediates. Overall, our work is one of the first quantitative investigations of the impact of the ancillary ligand, solvent, and LAs on CO_2 insertion into metal alkyl bonds and will assist in the development of improved and new catalysts for CO_2 utilization.

Results and discussion

Synthesis of $^{\mathrm{R}}$PBP supported nickel and palladium methyl complexes and reactivity with CO_2

Previous studies on CO_2 insertion into pincer supported group 10 metal hydrides demonstrate that the rate of CO_2 insertion increases as the *trans*-influence of the donor opposite to the hydride ligand increases.[19] As a result, nickel and palladium hydride complexes supported by $^{\mathrm{Cy}}$PSiP ($^{\mathrm{Cy}}$PSiP = Si(Me)(2-PCy_2-C_6H_4)$_2$) ligands, which contain a strongly donating silyl ligand *trans* to the hydride insert CO_2 more rapidly than the corresponding species containing $^{\mathrm{R}}$PCP ligands. We hypothesized

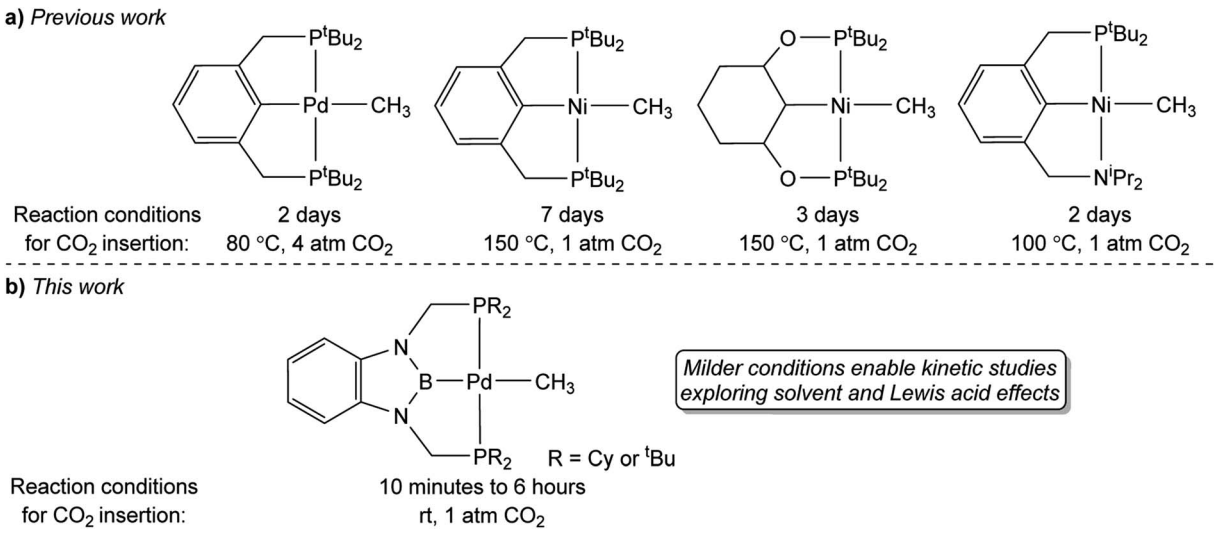

Fig. 1 (a) Previous examples of pincer-supported group 10 methyl complexes that undergo CO_2 insertion to form κ^1-acetate complexes. (b) $^{\mathrm{R}}$PBP supported palladium complexes studied in this work, which undergo CO_2 insertion under milder conditions.

that a similar trend may also occur for nickel and palladium methyl species. Unfortunately, the previously described complexes (^{Cy}PSiP)M(CH_3) (M = Ni or Pd) undergo an intramolecular ligand rearrangement,[20] as does (^{tBu}PSiP)Pd(CH_3) (^{tBu}PSiP = Si(Me)(2-P^{t}Bu$_2$-C$_6$H$_4$)$_2$, see ESI†) which complicates studies of CO_2 insertion. Therefore, we prepared nickel and palladium methyl complexes supported by ^{R}PBP ligands (^{R}PBP = B(NCH$_2$PR$_2$)$_2$C$_6$H$_4$; R = Cy or ^{t}Bu) that feature a boryl donor, which has previously been shown to exert a large *trans*-influence,[21] opposite the methyl ligand.

(^{Cy}PBP)Ni(CH_3) was synthesized *via* an analogous route to that previously described for (^{tBu}PBP)Ni(CH_3).[21h] Initially, $NiCl_2$·DME was treated with ^{Cy}PB^{H}P to generate (^{Cy}PBP)NiCl in 68% yield (Scheme 1). The subsequent reaction of (^{Cy}PBP)NiCl with MeMgCl generates (^{Cy}PBP)Ni(CH_3) in 26% yield. The major cause of the low yield of (^{Cy}PBP)Ni(CH_3) is the need to perform sequential recrystallizations to remove magnesium salts. Specifically, considerable care is required to remove $MgCl_2$ by-products from the Grignard reagent, which cause the methyl species to convert back to the chloride complex. (^{Cy}PBP)Ni(CH_3) was characterized in the solid-state using X-ray crystallography (Fig. 2) and has an analogous distorted square planar geometry to (^{tBu}PBP)Ni(CH_3).[21h] The P(1)–Ni(1)–P(2) bond angle is 158.67(10)°, which is similar to that observed in (^{tBu}PBP)Ni(CH_3) (157.58(2)°). The B(1)–Ni(1)–C(1) bond angle is almost linear (179.1(4)°), which presumably results in the boryl ligand exerting the maximum possible *trans*-influence on the methyl ligand. The Ni(1)–B(1) bond length in (^{Cy}PBP)Ni(CH_3) is 1.927(9) Å, which is comparable to other species with a Ni–boryl bond.[21h,22] The nickel methyl bond length is 2.019(9) Å, which is significantly shorter than the nickel methyl bond length in (^{tBu}PBP)Ni(CH_3), which is 2.059(2) Å. The longer bond length in (^{tBu}PBP)Ni(CH_3) is likely due to steric factors, as the larger steric properties of the *tert*-butyl substituents in (^{tBu}PBP)Ni(CH_3) may cause the nickel methyl bond to elongate. The increased steric demand of the ^{tBu}PBP ligand was confirmed using buried volume calculations (Samb*V*ca 2.1 (ref. 23)) using the crystal structures of (^{R}PBP)Ni(CH_3), which show that the buried volume of (^{tBu}PBP)Ni(CH_3) is 92.1% compared to 89.3% for (^{Cy}PBP)Ni(CH_3) (see ESI†).

Palladium chloride complexes supported by ^{R}PBP (R = Cy or ^{t}Bu) ligands were synthesized through the reaction of the protonated ^{R}PB^{H}P ligand with commercially available [(η^3-allyl)PdCl]$_2$ in yields of 69% and 63%, respectively. This is different to a previous route utilized to metallate the ^{tBu}PBP ligand, which used the more expensive Pd(COD)Cl_2 as the palladium source.[21k] Treatment of (^{R}PBP)PdCl with MeLi results in the formation of the (^{R}PBP)Pd(CH_3) in yields of 25% for (^{Cy}PBP)Pd(CH_3) and 60% for (^{tBu}PBP)Pd(CH_3) (Scheme 2). In an analogous fashion to (^{Cy}PBP)Ni(CH_3), it is important to remove alkali halide by-products as they can cause the palladium methyl species to be converted back to the palladium chloride precursor and the multiple recrystallizations required for (^{Cy}PBP)Pd(CH_3) lowers the yield. (^{tBu}PBP)Pd(CH_3) was characterized using X-ray crystallography (Fig. 3). The geometry around palladium is distorted square planar. The P(1)–Pd(1)–P(2) bond angle is 153.74(3)°, which is a greater deviation from linearity than that observed in a related complex with a ^{tBu}PCP ligand. Specifically in (^{tBu}PCP)PdCl P–Pd–P is 165.79(2)°.[24] As a consequence, the fourth coordination site in pincer complexes supported by ^{tBu}PBP is likely more sterically accessible than in species supported by ^{tBu}PCP ligands. The Pd(1)–B(1) bond length in (^{tBu}PBP)Pd(CH_3) is 2.027(4) Å, which is significantly longer than the Pd–B bond length in the only other crystallographically characterized palladium complex with a ^{tBu}PBP ligand, (^{tBu}PBP)PdCl (Pd–B is 1.972(4) Å). This is consistent with the methyl ligand exerting a significantly stronger *trans*-influence than the chloride ligand.

We treated complexes of the type (^{R}PBP)M(CH_3) (M = Ni or Pd, R = Cy or ^{t}Bu) with 1 atm of CO_2 in C_6D_6 at room

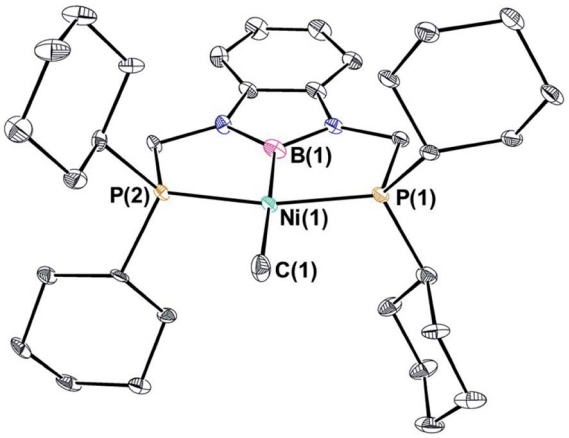

Fig. 2 Solid-state structure of (^{Cy}PBP)Ni(CH_3) with thermal ellipsoids at 30% probability. Hydrogen atoms are omitted for clarity. Selected distances (Å) and angles (°): Ni(1)–B(1) 1.927(9), Ni(1)–C(1) 2.019(9), Ni(1)–P(1) 2.148(2), Ni(1)–P(2) 2.138(2), B(1)–Ni(1)–C(1) 179.1(4), B(1)–Ni(1)–P(1) 80.1(3), C(1)–Ni(1)–P(1) 100.6(3), B(1)–Ni(1)–P(2) 78.7(3), C(1)–Ni(1)–P(2) 100.6(3), P(1)–Ni(1)–P(2) 158.67(10).

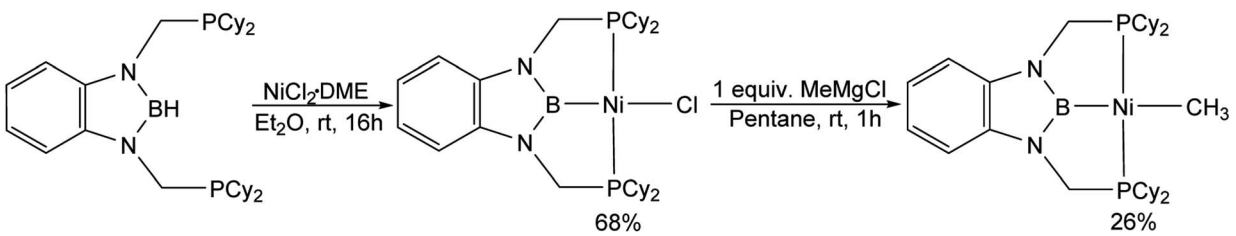

Scheme 1 Synthesis of (^{Cy}PBP)Ni(CH_3).

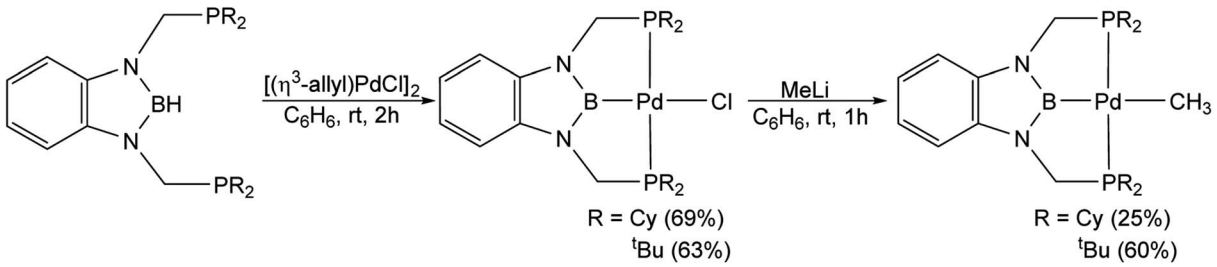

Scheme 2 Synthesis of (^{R}PBP)Pd(CH_3) (R = Cy or ^{t}Bu).

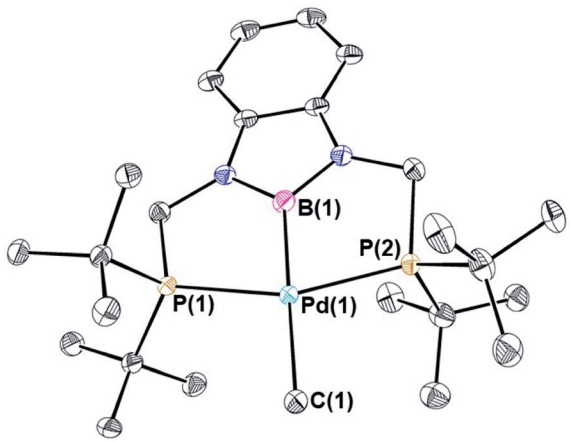

Fig. 3 Solid-state structure of (^{tBu}PBP)Pd(CH_3) with thermal ellipsoids at 30% probability. Hydrogen atoms are omitted for clarity. Selected distances (Å) and angles (°): Pd(1)–B(1) 2.027(4), Pd(1)–C(1) 2.185(4), Pd(1)–P(1) 2.3030(8), Pd(1)–P(2) 2.3035(8), B(1)–Pd(1)–C(1) 178.09(15), B(1)–Pd(1)–P(1) 77.36(12), C(1)–Pd(1)–P(1) 103.49(10), B(1)–Pd(1)–P(2) 77.33(12), C(1)–Pd(1)–P(2) 102.02(10), P(1)–Pd(1)–P(2) 153.74(3).

temperature (Scheme 3). In the cases of (^{R}PBP)Pd(CH_3) (R = Cy or ^{t}Bu) NMR spectroscopy indicated clean and essentially quantitative CO_2 insertion to the corresponding acetate complexes at room temperature. The reactions took 1 and 6 hours to reach completion for (^{Cy}PBP)Pd(CH_3) and (^{tBu}PBP)Pd(CH_3), respectively. These are the most rapid insertions of CO_2 into pincer-supported group 10 metal alkyl complexes observed to date. The acetate products were isolated and (^{tBu}PBP)Pd{OC(O)CH_3} was characterized using X-ray crystallography (Fig. 4). The solid-state structure of (^{tBu}PBP)Pd{OC(O)CH_3} has the same distorted square planar geometry as (^{tBu}PBP)Pd(CH_3) and confirms κ^1-binding of the acetate. As expected, the Pd(1)–B(1) bond length (1.975(2) Å) in (^{tBu}PBP)Pd{OC(O)CH_3} is significantly shorter than the Pd–B bond length in (^{tBu}PBP)Pd(CH_3) (2.027(4) Å) due to the weaker *trans*-influence of the acetate ligand. Further, the increased Pd–O bond length in (^{tBu}PBP)Pd{OC(O)CH_3} (2.1861(14) Å) in comparison to (^{tBu}PCP)Pd{OC(O)CH_3} (2.1279(19) Å)[15] is consistent with the increased *trans*-influence of the ^{tBu}PBP ligand in comparison to the related ^{tBu}PCP ligand. In contrast, the insertion of CO_2 into (^{Cy}PBP)Ni(CH_3) was not clean. Although NMR spectroscopy suggested that (^{Cy}PBP)Ni{OC(O)CH_3}, which was not isolated, was the major product, free ligand and several unidentified decomposition products were present (see ESI†). Additionally, it took approximately 4 days at room temperature for all of the (^{Cy}PBP)Ni(CH_3) to disappear. Overall, from these initial qualitative examples of CO_2 insertion into (^{Cy}PBP)M(CH_3) (M = Ni or Pd) and (^{tBu}PBP)Pd(CH_3) we can make the following conclusions: (i) the insertion of CO_2 into (^{Cy}PBP)Pd(CH_3) is faster than the corresponding insertion into (^{Cy}PBP)Ni(CH_3). This is in agreement with results for CO_2 insertion into (^{tBu}PCP)M(CH_3) (M = Ni or Pd)[15,16] but stands in contrast to computational studies of CO_2 insertion into (^{tBu}PCP)MH (M = Ni or Pd), where insertion is proposed to be faster for nickel.[19] (ii) The insertion of CO_2 into (^{tBu}PBP)Pd(CH_3) is significantly faster than the corresponding insertion into (^{tBu}PCP)Pd(CH_3).[15] This suggests that the rate of CO_2 insertion can be increased by having a stronger *trans*-influence donor opposite the methyl, similar to what has been observed for CO_2 insertion into group 10 metal hydrides.[19] (iii) The faster insertion of CO_2 into (^{Cy}PBP)Pd(CH_3) compared to (^{tBu}PBP)Pd(CH_3) suggests that steric factors are important.

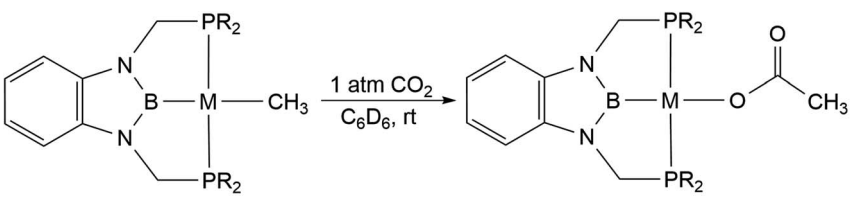

Scheme 3 Generation of (^{R}PBP)M{OC(O)CH_3} (M = Ni, R = Cy; M = Pd, R = Cy or ^{t}Bu) through CO_2 insertion into (^{R}PBP)M(CH_3).

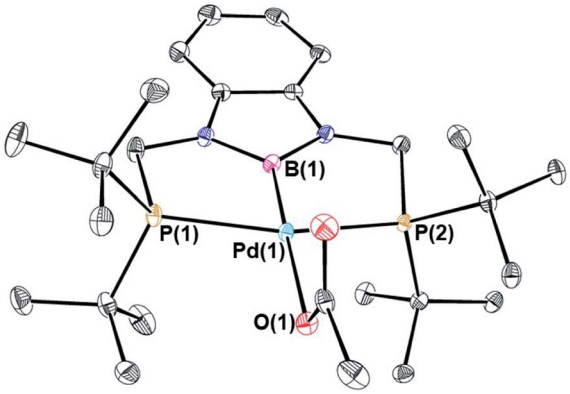

Fig. 4 Solid-state structure of ($^{t\mathrm{Bu}}$PBP)Pd{OC(O)CH$_3$} with thermal ellipsoids at 30% probability. Hydrogen atoms are omitted for clarity. Selected distances (Å) and angles (°): Pd(1)–B(1) 1.975(2), Pd(1)–O(1) 2.1861(14), Pd(1)–P(1) 2.3256(5), Pd(1)–P(2) 2.3336(5), B(1)–Pd(1)–O(1) 174.99(7), B(1)–Pd(1)–P(1) 77.32(7), O(1)–Pd(1)–P(1) 100.17(4), B(1)–Pd(1)–P(2) 79.00(7), O(1)–Pd(1)–P(2) 103.05(4), P(1)–Pd(1)–P(2) 155.805(18).

In contrast to the quantitative or relatively clean insertion of CO_2 observed for ($^{\mathrm{Cy}}$PBP)Pd(CH$_3$), ($^{t\mathrm{Bu}}$PBP)Pd(CH$_3$), and ($^{\mathrm{Cy}}$PBP)Ni(CH$_3$), insertion into ($^{t\mathrm{Bu}}$PBP)Ni(CH$_3$) was not clean and was significantly slower than for the other methyl compounds. After 10 days at room temperature, approximately 30% of ($^{t\mathrm{Bu}}$PBP)Ni(CH$_3$) was still observed, along with 50% of a product we propose to be ($^{t\mathrm{Bu}}$PBP)Ni{OC(O)CH$_3$} on the basis of its similar ^{31}P NMR chemical shift to ($^{\mathrm{Cy}}$PBP)Ni{OC(O)CH$_3$}, and 20% of unidentified decomposition products (Scheme 4). Attempts to independently synthesize ($^{t\mathrm{Bu}}$PBP)Ni{OC(O)CH$_3$} *via* reactions between silver acetate and ($^{t\mathrm{Bu}}$PBP)NiCl or sodium acetate and ($^{t\mathrm{Bu}}$PBP)Ni(OTf) were unsuccessful. Although, initially a new resonance is observed in the ^{31}P NMR spectra of these reactions with the same chemical shift as the proposed insertion product with CO_2 (84.9 ppm), this resonance disappears over time, indicating that ($^{t\mathrm{Bu}}$PBP)Ni{OC(O)CH$_3$} is likely unstable in solution. This decomposition prohibited isolation and full characterization of ($^{t\mathrm{Bu}}$PBP)Ni{OC(O)CH$_3$}. Nevertheless, since the rate of CO_2 insertion into ($^{t\mathrm{Bu}}$PBP)Ni(CH$_3$) is presumably independent of the decomposition of the corresponding insertion product, we can make qualitative conclusions about the rate of insertion. We hypothesize that the slower rate of CO_2 insertion is related to the increased steric bulk of ($^{t\mathrm{Bu}}$PBP)Ni(CH$_3$), which makes it harder for CO_2 to interact with the complex. When ($^{t\mathrm{Bu}}$PBP)Ni(CH$_3$) was treated with CO_2 at higher temperatures even larger amounts of decomposition products were observed. Control experiments indicate that ($^{t\mathrm{Bu}}$PBP)Ni(CH$_3$) is not stable even when heated under an N_2 atmosphere. Although we were unable to identify all of the decomposition products of ($^{t\mathrm{Bu}}$PBP)Ni(CH$_3$), an unusual dinuclear species ($^{t\mathrm{Bu}}$PB$^{\mathrm{Me}}$P)$_2$Ni$_2$(μ-N$_2$) ($^{t\mathrm{Bu}}$PB$^{\mathrm{Me}}$P = MeB(NCH$_2$P^{t}Bu$_2$)$_2$-C$_6$H$_4$), containing two nickel(0) centers and a bridging dinitrogen ligand crystallized out of solution (Fig. 5). In this complex, the nickel methyl ligand has undergone reductive coupling with the boryl ligand to form a new C–B bond. The boron atom no longer coordinates to the nickel center and the two phosphorus donors of the new bidentate $^{t\mathrm{Bu}}$PB$^{\mathrm{Me}}$P ligands do not coordinate to the same nickel center but instead coordinate to two different nickel atoms. The geometry around the nickel centers is distorted trigonal planar and the dinitrogen ligand coordinates in an end-on fashion. The N–N bond distance of 1.145(8) Å is slightly elongated compared to that of free N_2 (1.098 Å), consistent with weak activation of N_2 and what has been observed in related nickel dinitrogen complexes.[25] The decomposition of ($^{t\mathrm{Bu}}$PBP)Ni(CH$_3$) into ($^{t\mathrm{Bu}}$PB$^{\mathrm{Me}}$P)$_2$Ni$_2$(μ-N$_2$) demonstrates a new reductive pathway for decomposition of complexes supported by $^{\mathrm{R}}$PBP ligands. However, this is likely a particular problem for the $^{t\mathrm{Bu}}$PBP ligand when it is coordinated to Ni because of steric constraints associated with the bulky *tert*-butyl substituents and small size of nickel.

Kinetic studies of CO_2 insertion into ($^{t\mathrm{Bu}}$PBP)Pd(CH$_3$). It has traditionally been challenging to perform kinetics experiments on CO_2 insertion into group 10 alkyl complexes either because of the instability of the complexes[14] or the harsh conditions required for insertion.[16,17] In contrast, the insertion of CO_2 into ($^{t\mathrm{Bu}}$PBP)Pd(CH$_3$) under mild conditions enables kinetics experiments to be performed. Initially, ^{1}H or ^{31}P NMR spectroscopy was used to monitor the reaction of ($^{t\mathrm{Bu}}$PBP)Pd(CH$_3$) with CO_2 as a function of time (Fig. 6a). It was possible to measure the concentrations of both the ($^{t\mathrm{Bu}}$PBP)Pd(CH$_3$) starting material and the ($^{t\mathrm{Bu}}$PBP)Pd{OC(O)CH$_3$} product, which enabled us to confirm the reaction is clean and quantitative. An excess of CO_2 was used to ensure that the reactions were performed under pseudo-first order conditions with the concentration of CO_2 measured using quantitative ^{13}C NMR spectroscopy (see SI).[26] Initial experiments in C$_6$D$_6$ indicate that the reaction is first order in both [($^{t\mathrm{Bu}}$PBP)Pd(CH$_3$)] and [CO_2], demonstrating that the overall rate law is k_1[($^{t\mathrm{Bu}}$PBP)Pd(CH$_3$)][CO_2] (Fig. 6b and 7). The k_{obs} values obtained from a plot of ln([($^{t\mathrm{Bu}}$PBP)Pd(CH$_3$)])

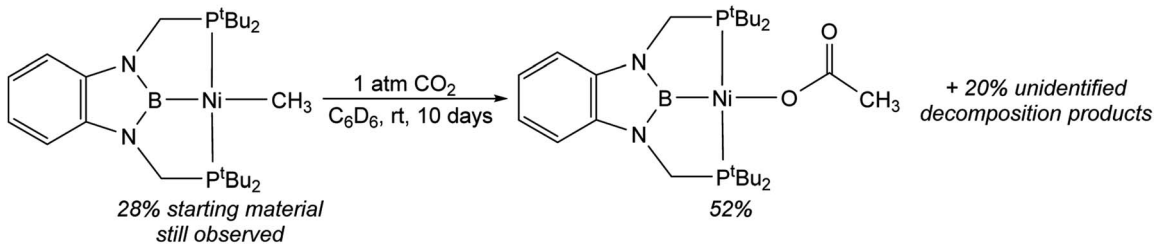

Scheme 4 CO_2 insertion into ($^{t\mathrm{Bu}}$PBP)Ni(CH$_3$).

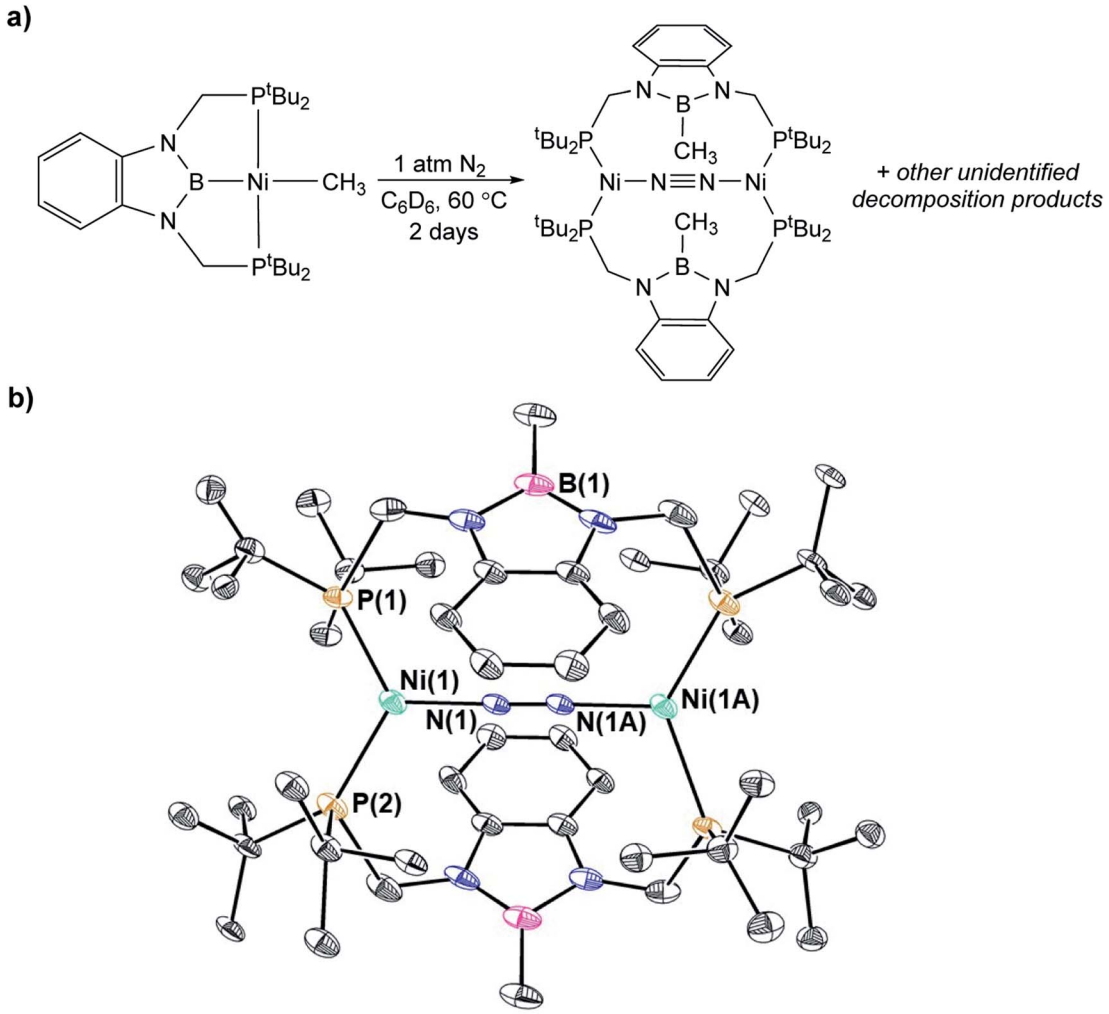

Fig. 5 a) Decomposition of (^{tBu}PBP)Ni(CH$_3$) under N$_2$ at 60 °C. (b) Solid-state structure of (^{tBu}PB^{Me}P)$_2$Ni$_2$(μ-N$_2$) with thermal ellipsoids at 30% probability. The model is near the crystallographic inversion center; half of the structure is generated by symmetry. Hydrogen atoms are omitted for clarity. Selected distances (Å) and angles (°): Ni(1)–N(1) 1.854(4), Ni(1)–P(1) 2.293(11), Ni(1)–P(2) 2.164(11), N(1)–N(1A) 1.145(8), P(1)–Ni(1)–P(2) 122.0(5), N(1)–Ni(1)–P(1) 118.9, N(1)–Ni(1)–P(2) 110.8(3), Ni(1)–N(1)–N(1A) 178.7(5).

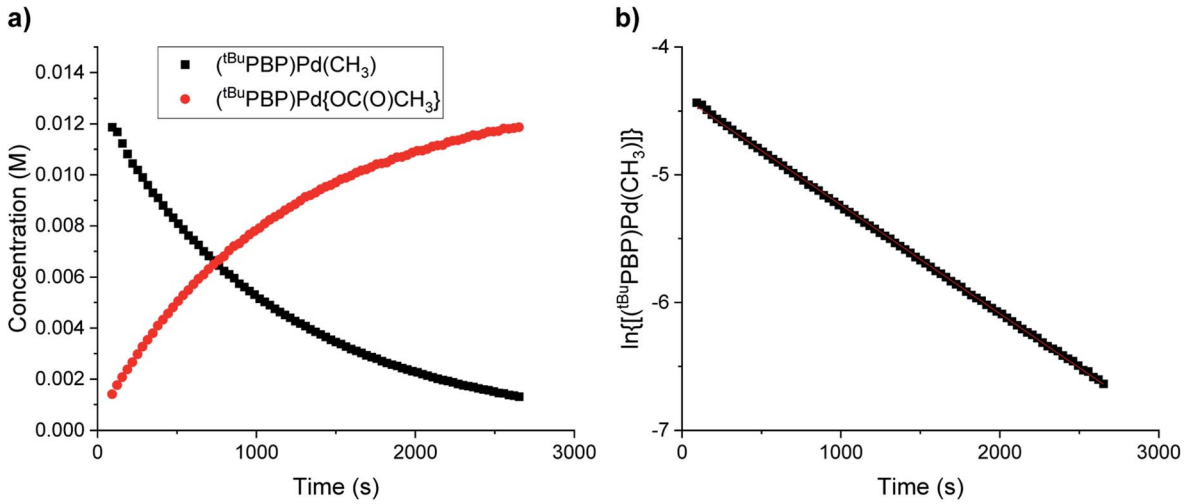

Fig. 6 Representative traces for the insertion of CO$_2$ into (^{tBu}PBP)Pd(CH$_3$) at 40 °C in C$_6$D$_6$ with 1 atm of CO$_2$ showing (a) the concentrations of (^{tBu}PBP)Pd(CH$_3$) and (^{tBu}PBP)Pd{OC(O)CH$_3$} as a function of time and (b) the ln of the concentration of (^{tBu}PBP)Pd(CH$_3$) as a function of time.

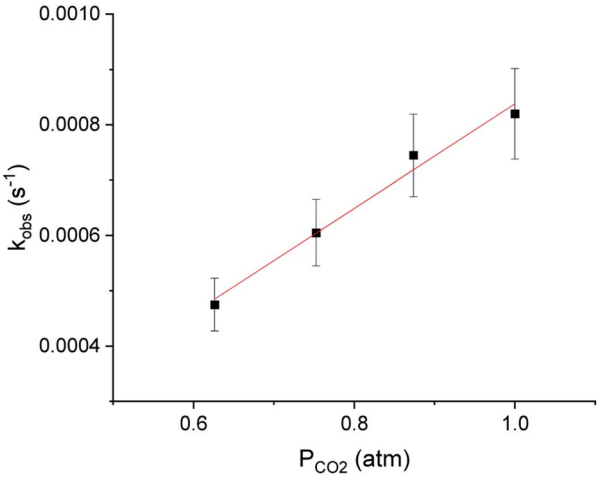

Fig. 7 Reaction order in [CO_2] of the insertion of CO_2 into ($^{t\text{Bu}}$PBP)Pd(CH_3) in C_6D_6 at 40 °C.

versus time were divided by the concentration of CO_2 to obtain values of k_1 (see ESI†). Monitoring the rate of the reaction in C_6D_6 at various temperatures allowed for the activation parameters to be determined through Eyring analysis (see ESI†). The enthalpy of activation, $\Delta H^{\ddagger}$, 10.9 ± 1.1 kcal mol^{-1}, for insertion into ($^{t\text{Bu}}$PBP)Pd(CH_3) is significantly lower than that for ($^{t\text{Bu}}$PCP)Pd(CH_3) ($\Delta H^{\ddagger}$ = 17.4 ± 1.7 kcal mol^{-1}),[26] which is the most closely related system for which an experimental activation energy for CO_2 insertion has been measured. This is consistent with the hypothesis that the strong *trans*-influence of the $^{t\text{Bu}}$PBP ligand weakens the palladium methyl bond and destabilizes the ground state. The entropies of activation, $\Delta S^{\ddagger}$, for ($^{t\text{Bu}}$PBP)Pd(CH_3) and ($^{t\text{Bu}}$PCP)Pd(CH_3) are within error of each other at −32.2 ± 3.2 and −28.2 ± 4.54 cal mol^{-1} K^{-1}, respectively. The similar negative values suggest that the nature of the rate-limiting transition state in both reactions are analogous and is in agreement with two molecules combining to form one molecule in the transition state (*vide infra*). The overall difference in $\Delta G^{\ddagger}$ at 298 K between ($^{t\text{Bu}}$PBP)Pd(CH_3) (20.5 ± 2.1 kcal mol^{-1}) and ($^{t\text{Bu}}$PCP)Pd(CH_3) (25.8 ± 2.6 kcal mol^{-1}) is consistent with the much faster rate of insertion observed for the $^{t\text{Bu}}$PBP system.

In CO_2 insertion reactions into metal hydrides, it has been demonstrated that the solvent can have a major influence on the rate of insertion.[5] To date there are no studies exploring how the rate of CO_2 insertion into metal alkyls varies as the solvent is changed. We determined the rate of CO_2 insertion (k_1) into ($^{t\text{Bu}}$PBP)Pd(CH_3) in toluene-d_8, benzene-d_6, 1,4-dioxane, THF, and glyme (Table 1). There was only a small solvent effect with approximately a 1.9-fold difference in k_1 between the slowest (toluene-d_8) and fastest (glyme) solvent (Table 1). This compares with a 30-fold increase in the rate of CO_2 insertion into an iridium hydride in a similar set of solvents.[5a] We propose that the smaller impact of solvent in this case is because there is less build-up of charge in the rate-determining transition state for CO_2 insertion (*vide infra*) compared to the corresponding transition state for metal hydrides. To determine if the variation in the rate of insertion correlated with any solvent parameters, ln(k_1) was plotted against the dielectric constant, Gutmann Acceptor Number (AN),[27] or Dimroth–Reichardt $E_T(30)$ parameter[18] of the solvent. No significant correlation was observed between the rate of CO_2 insertion and the dielectric constant or AN of a solvent (see ESI†). In contrast, an excellent correlation was observed between the $E_T(30)$ value of a solvent and the rate of CO_2 insertion (Fig. 8), suggesting that $E_T(30)$ is a good predictor of the rate of CO_2 insertion. A similar relationship was observed for CO_2 insertion into metal hydrides and hydroxides,[5b] raising the possibility that this correlation is general across a variety of distinct metal-element σ-bonds. It is likely that $E_T(30)$ is a better predictor of CO_2 insertion rates because it explicitly considers specific solute/solvent interactions, which are not accounted for when the solvent is modelled using either dielectric constant or AN.[5b] Unfortunately, we were unable to extend the correlation between the rate of CO_2 insertion into ($^{t\text{Bu}}$PBP)Pd(CH_3) and $E_T(30)$ to more polar solvents. This is

Table 1 Effect of solvent on rate of CO_2 insertion into ($^{t\text{Bu}}$PBP)Pd(CH_3) at 40 °C and 1 atm of CO_2

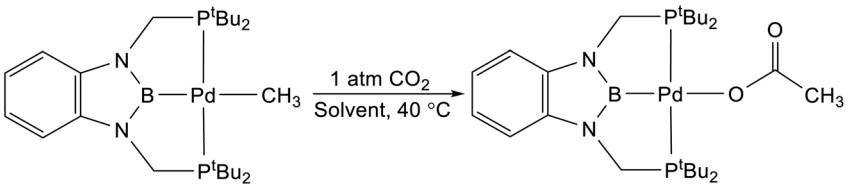

Entry	Solvent	k_1[a] (M^{-1} s^{-1} × 10^{-2})	Rate enhancement
1	Toluene-d_8	1.1	1
2	Benzene-d_6	1.3	1.2
3	1,4-Dioxane	1.5	1.4
4	Tetrahydrofuran	1.8	1.6
5	Glyme	2.1	1.9

[a] These values are the average of two trials and the errors are ±10%.

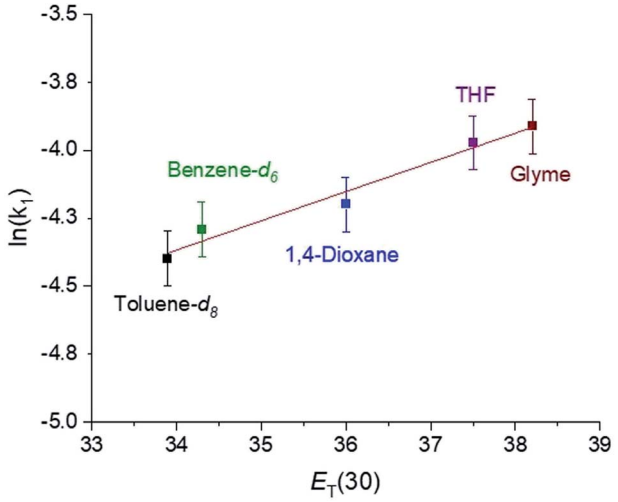

Fig. 8 Plot of ln(k_1) for the insertion of CO_2 into ($^{t\text{Bu}}$PBP)Pd(CH_3) *versus* the Dimroth–Reichardt $E_T(30)$ solvent parameter for various solvents at 40 °C and 1 atm of CO_2.

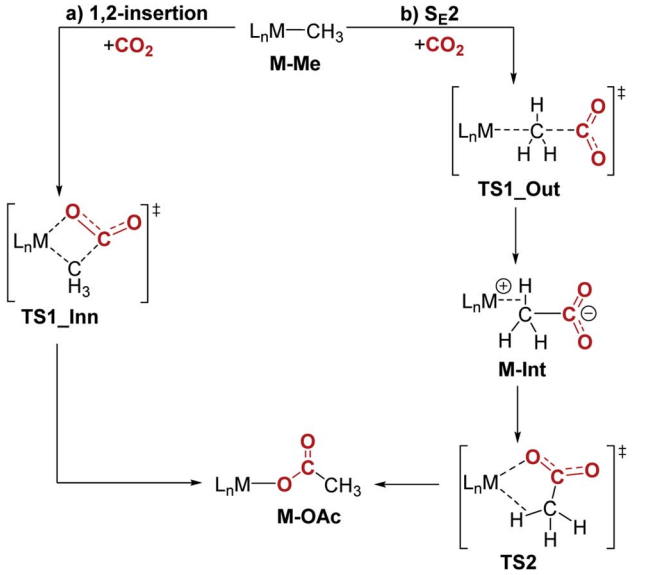

Fig. 9 Two plausible mechanisms for CO_2 insertion into pincer-supported group 10 methyls: (a) 1,2-insertion and (b) S_E2.

because these solvents led to the decomposition of ($^{t\text{Bu}}$PBP)Pd(CH_3) or resulted in rates that were too fast to measure using NMR spectroscopy. For example, CO_2 insertion into ($^{t\text{Bu}}$PBP)Pd(CH_3) is complete in less than 10 minutes at room temperature in pyridine and benzonitrile, which is too fast to obtain reliable kinetics by NMR spectroscopy. Nevertheless, given the slow rates of CO_2 insertion previously observed into pincer-supported group 10 alkyls, the completion of reactions in less than 10 minutes at room temperature is unprecedented.

Lewis acids have been proposed to increase the rate of CO_2 insertion into a variety of different metal-element σ-bonds, but these effects are often dependent on the pathway of insertion and the reaction conditions.[5,7,8,9b,28] As a result, it is difficult to predict when a Lewis acid will increase the rate of a CO_2 insertion reaction. We evaluated the impact of a variety of different Lewis acids on the rate of CO_2 insertion into ($^{t\text{Bu}}$PCP)Pd(CH_3) using THF as the solvent (Table 2).[29] Although there is an increase in rate when the reaction was performed in the presence of 20 equivalents of a variety of Lewis acids, a control experiment using 20 equivalents of (^{n}Bu$_4$)PF_6, which does not contain a Lewis acid, gives the same enhancement. This indicates that there is no increase in rate caused by Lewis acids and instead it is likely the case that increasing the ionic strength of the solution results in a slight enhancement in the rate of CO_2 insertion. Consistent with this hypothesis, all of the different Lewis acids evaluated give approximately the same increase in the rate of CO_2 insertion. At this stage, it is unclear why no Lewis

Table 2 Effect of Lewis acids on rate of CO_2 insertion into ($^{t\text{Bu}}$PBP)Pd(CH_3) in THF at 40 °C and 1 atm of CO_2

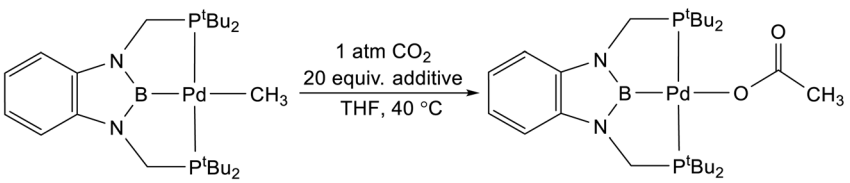

Entry	Additive (20 equiv.)	k_{obs} [b] ($s^{-1} \times 10^{-3}$)	Rate enhancement
1	None	1.6	1
2	(NBu_4)PF_6	2.3	1.4
3	$LiNTf_2$ [a]	2.2	1.4
4	$NaNTf_2$ [a]	2.1	1.3
5	$KNTf_2$ [a]	2.3	1.4
6	$LiPF_6$	2.4	1.5
7	$LiBPh_4 \cdot 3DME$	2.5	1.6
8	LiOTf	2.1	1.3

[a] NTf = triflimide. [b] These values are the average of two trials and the errors are ±10%.

acid effect is observed in the insertion of CO_2 into (^{tBu}PBP)Pd(CH_3), given that Li^+ has been demonstrated to increase the rate of CO_2 insertion into $(CO)_5W(CH_3)$.[8] However, in the next section, DFT calculations are performed to understand the exact nature of the transition states involved in CO_2 insertion into (^{tBu}PBP)Pd(CH_3).

Computational studies of CO_2 insertion into (^{R}PBP)Pd(CH_3) and related species. Previous studies investigating CO_2 insertion into PCP-supported palladium and nickel methyl complexes have proposed two plausible pathways for insertion: (i) a 1,2-insertion (inner sphere) or (ii) an S_E2 pathway (outer sphere).[16,17c,26] In the 1,2-insertion pathway, the O-bound acetate product is formed in one step and CO_2 interacts with the metal in the key transition state (Fig. 9a). This means that both the C–C and M–O bonds are formed at the same time. In contrast, the S_E2 pathway involves two steps and starts with electrophilic attack of CO_2 on the coordinated methyl, without any direct interaction between CO_2 and the metal (Fig. 9b). This results in

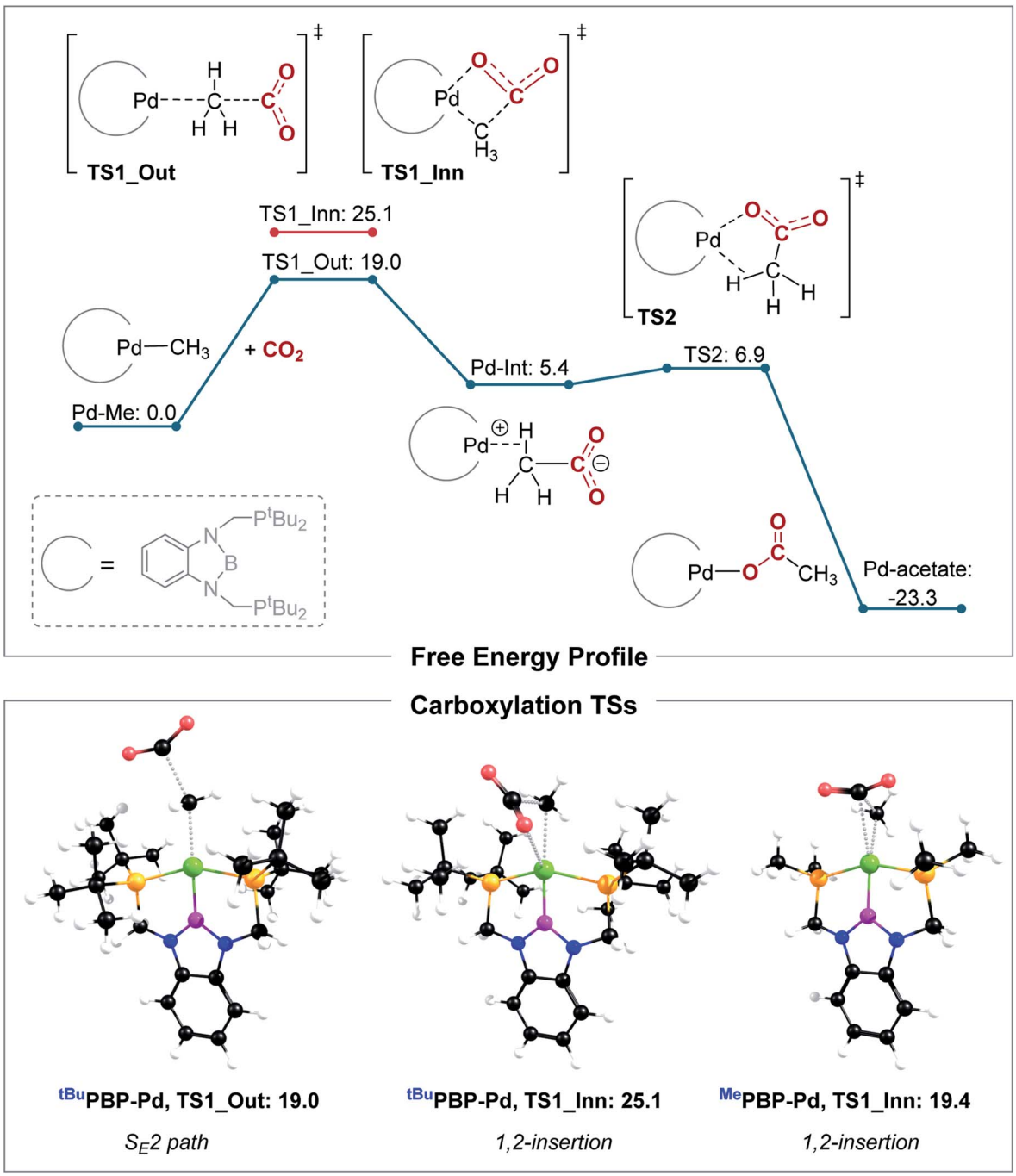

Fig. 10 Top: computed free energy profile (B3LYP-D3/def2-TZVPPD[CPCM]//B3LYP-D3/def2-SVP[CPCM], 298 K) for CO_2 insertion into (^{tBu}PBP)Pd(CH_3), bottom: optimized transition state structures for CO_2 insertion into (^{R}PBP)Pd(CH_3), with R = ^{t}Bu or Me. All energies are in kcal mol^{-1}.

Table 3 Calculated free energy barriers for inner and outer sphere C–CO_2 bond formation with different pincer-supported palladium and nickel complexes (kcal mol^{-1}, B3LYP-D3/def2-TZVPPD[CPCM]//B3LYP-D3/def2-SVP[CPCM], 298 K)[a]

Complex	**TS1_Out** (kcal mol^{-1})	**TS1_Inn** (kcal mol^{-1})
($^{t\text{Bu}}$PBP)Pd(CH_3)	**19.0** (23.9)	25.1 (30.6)
($^{\text{Me}}$PBP)Pd(CH_3)	22.5 (23.4)	**19.4** (21.0)
($^{t\text{Bu}}$PBP)Ni(CH_3)	**24.5** (27.8)	31.9 (33.7)
($^{t\text{Bu}}$PCP)Pd(CH_3)	**24.2** (29.2)	36.7 (41.1)
($^{\text{Me}}$PCP)Pd(CH_3)	26.8 (30.0)	**25.0** (27.8)

[a] For comparison, results for the ωB97XD functional are given in parenthesis, showing the same mechanistic trends.

the formation of the new C–C bond. In the second step, the intermediate containing an acetate-metal ion-pair rearranges *via* TS2 to form the O-bound acetate adduct. Here, we used DFT methods to understand the pathway for CO_2 insertion into ($^{t\text{Bu}}$PBP)M(CH_3) (M = Ni or Pd). We also independently calculated CO_2 insertion into ($^{t\text{Bu}}$PCP)Pd(CH_3) in order to directly compare it with the $^{t\text{Bu}}$PBP systems.

Our calculations indicate that CO_2 insertion into ($^{t\text{Bu}}$PBP)Pd(CH_3) proceeds *via* an S_E2 pathway (Fig. 10, S43, S44† & Table 3). The rate-limiting step is the initial attack of CO_2 on the palladium methyl group (**TS1_Out**), which has a computed barrier of 19.0 kcal mol^{-1} (298 K). This is within error of the activation barrier measured experimentally (*vide supra*). Although there is no interaction between CO_2 and the metal in **TS1_Out**, we note that there are two C–H…OCO interactions between the *tert*-butyl substituents of the $^{t\text{Bu}}$PBP ligand and CO_2 (2.43 and 2.74 Å, respectively), which provide charge stabilization. This may explain why the addition of Lewis acids to the system does not result in a rate enhancement (*vide supra*). The second step of the S_E2 pathway has a very small barrier and involves rotation of the acetate-palladium ion pair to form the O-bound acetate product (Fig. 10). In contrast, the barrier for the alternative 1,2-insertion is significantly higher at 25.1 kcal mol^{-1} (**TS1_Inn**, Fig. 10 and S45†). The high barrier is likely caused by the bulky *tert*-butyl substituents of the $^{t\text{Bu}}$PBP ligand, which make it difficult for CO_2 to approach palladium without steric repulsion. In order to investigate this hypothesis, we calculated CO_2 insertion into ($^{\text{Me}}$PBP)Pd(CH_3), where the *tert*-butyl substituents on the $^{t\text{Bu}}$PBP ligand have been replaced with methyl substituents. For CO_2 insertion into ($^{\text{Me}}$PBP)Pd(CH_3) the 1,2-insertion pathway is preferred by 3.1 kcal mol^{-1} over the S_E2 mechanism (Fig. 10, S46 and S47†). Thus, the size of the pincer ligand has a decisive role in promoting either a 1,2-insertion (small phosphine substituents) or an S_E2 pathway (large phosphine substituents). Similar ligand effects were previously observed for NHC–Cu complexes.[30]

The $^{t\text{Bu}}$PCP-supported complex, ($^{t\text{Bu}}$PCP)Pd(CH_3), also shows a preference for the S_E2 pathway, with a computed barrier of 24.2 kcal mol^{-1} (**TS_Out**, Fig. S48 and S49†). Consistent with previous results,[26] the 1,2-insertion mechanism is unlikely for ($^{t\text{Bu}}$PCP)Pd(CH_3) due to the high barrier of 36.7 kcal mol^{-1} (**TS_Inn**, Fig. S50†).[31] Thus, both ($^{t\text{Bu}}$PBP)Pd(CH_3) and ($^{t\text{Bu}}$PCP)Pd(CH_3) show a clear preference for an S_E2 mechanism. In the rate limiting transition state (**TS_Out**), ($^{t\text{Bu}}$PBP)Pd(CH_3) displays a longer C–CO_2 bond (by 0.09 Å) and a smaller CO_2 angle (by 1.7°) compared to ($^{t\text{Bu}}$PCP)Pd(CH_3), which indicates an earlier TS. The lower barrier for ($^{t\text{Bu}}$PBP)Pd(CH_3) (by 5.2 kcal mol^{-1}) is in agreement with our kinetic studies, showing that CO_2 insertion is much faster for ($^{t\text{Bu}}$PBP)Pd(CH_3). The decrease in the barrier for CO_2 insertion is also matched by the greater thermodynamic driving force for CO_2 insertion into ($^{t\text{Bu}}$PBP)Pd(CH_3) compared with ($^{t\text{Bu}}$PCP)Pd(CH_3) (−23.3 kcal mol^{-1} *versus* −15.8 kcal mol^{-1}). These results highlight how a donor atom with strong *trans*-influence opposite to the methyl can lower the barrier for insertion and suggest that the enhancement is due to destabilization of the ground state as opposed to a kinetic effect associated with stabilization of the transition state.

The slower qualitative rate of CO_2 insertion into ($^{t\text{Bu}}$PBP)Ni(CH_3) compared to ($^{t\text{Bu}}$PBP)Pd(CH_3) (*vide supra*) is surprising given that CO_2 insertion into nickel hydrides is typically faster than palladium hydrides.[19] Calculations on CO_2 insertion into ($^{t\text{Bu}}$PBP)Ni(CH_3) confirm our experimental results as the calculated barrier is 24.5 kcal mol^{-1} at 298 K, more than 5 kcal mol^{-1} higher than for ($^{t\text{Bu}}$PBP)Pd(CH_3) (B3LYP-D3, Table 3). The lowest energy pathway for CO_2 insertion into ($^{t\text{Bu}}$PBP)Ni(CH_3) also follows an S_E2 mechanism (Fig. S51 and 52†). Geometrical analysis of the rate-determining transition states for CO_2 insertion into ($^{t\text{Bu}}$PBP)Ni(CH_3) and ($^{t\text{Bu}}$PBP)Pd(CH_3) shows that the Ni–P bonds are shorter by around 0.15 Å compared with the corresponding Pd–P bonds due to the smaller atomic radius of nickel. We propose that the increased steric congestion around nickel results in the higher barrier for CO_2 insertion relative to the palladium system.[32] This is in agreement with previous results showing that CO_2 insertion reactions into nickel hydrides are highly sensitive to steric factors.[5a] It is likely, however, that there is no inherent electronic reason for CO_2 insertion into nickel methyl complexes to be slower than palladium methyl complexes, and if a nickel complex could be prepared where steric factors were not relevant,[33] we expect to see comparable rates of insertion.

Conclusions

In this work, we have demonstrated that nickel and palladium methyl complexes supported by $^{\text{R}}$PBP ligands undergo CO_2 insertion under significantly milder conditions than any previously reported pincer-ligated group 10 alkyl species. This is because of the strong *trans*-influence of the central boryl donor in $^{\text{R}}$PBP type ligands, which destabilizes the M–CH_3 bond. Qualitatively, we show that CO_2 insertion into ($^{\text{R}}$PBP)Pd(CH_3) is faster than CO_2 insertion into ($^{\text{R}}$PBP)Ni(CH_3), which is likely due to steric factors. In contrast, we propose that steric factors are less significant in CO_2 insertion into group 10 hydrides, and as a result nickel hydrides typically undergo faster insertion than palladium hydrides.[19] Given the rapid rate of insertion into $^{\text{R}}$PBP-ligated complexes, we were able to complete a rare kinetic study on CO_2 insertion into a metal alkyl complex. Our results demonstrate that the solvent parameter that is best for

predicting the rate of CO_2 insertion is the Dimroth–Reichardt $E_T(30)$ parameter. This is analogous to what we have observed for transition metal hydrides,[5b] but the dependence of the insertion rate on the solvent is significantly less pronounced in the case of the metal alkyl complex. We hypothesize that this is because there is less charge build-up in the transition state for carbon dioxide insertion into a metal alkyl complex compared to related metal hydrides. Consistent with there being only a small build-up of charge in the transition state, we did not observe any enhancement from Lewis acids in CO_2 insertion reactions into (^{tBu}PBP)Pd(CH_3). DFT calculations indicate that the proposed mechanism for insertion into (^{tBu}PBP)M(CH_3) (M = Ni or Pd) follows an S_E2 pathway, but this is dependent on steric factors and compounds with less bulky substituents on the phosphine donors are more likely to undergo insertion *via* a 1,2-insertion mechanism. Overall, our results indicate that the fastest systems for CO_2 insertion into a group 10 methyl will have a strong *trans*-influence donor opposite the methyl, be able to undergo insertion in solvents with high $E_T(30)$ values, and not have sterically bulky ancillary ligands that prevent the approach of CO_2. Future research in our group will aim to extend these principles to other metal-element σ-bonds and apply them to improve catalytic reactions.

Data availability

Additional information about selected experiments, NMR spectra, and other details are availabe *via* the internet.

Author contributions

Project conception: AJD, MRE, DJC, NH; experimental work: AJD, MRE, DJC; X-ray crystallography: BQM; computational analysis: LjP, KHH. All authors contributed to writing the manuscript.

Conflicts of interests

The authors declare no competing financial interests.

Acknowledgements

NH acknowledges support from National Science Foundation through Grant CHE-1953708. We thank Dr Hee Won Suh for preliminary work on this project and Dr Fabian Menges for assistance obtaining high resolution mass spectrometry data with equipment funded by NSF MRI Grant CHE-1828190. KHH and LjP thank the Research Council of Norway (Grant No. 300769), the Tromsø Research Foundation (Grant No. TFS2016KHH), NordForsk (Grant No. 85378) and Sigma2 - the National Infrastructure for High Performance Computing and Data Storage in Norway (No. nn9330k).

References

1 (*a*) E. A. Quadrelli, G. Centi, J.-L. Duplan and S. Perathoner, Carbon Dioxide Recycling: Emerging Large-Scale Technologies with Industrial Potential, *ChemSusChem*, 2011, **4**, 1194–1215; (*b*) J. Schneider, H. Jia, J. T. Muckerman and E. Fujita, Thermodynamics and Kinetics of CO_2, CO, and H^+ Binding to the Metal Centre of CO_2 Reduction Catalysts, *Chem. Soc. Rev.*, 2012, **41**, 2036–2051; (*c*) A. M. Appel, J. E. Bercaw, A. B. Bocarsly, H. Dobbek, D. L. DuBois, M. Dupuis, J. G. Ferry, E. Fujita, R. Hille, P. J. A. Kenis, C. A. Kerfeld, R. H. Morris, C. H. F. Peden, A. R. Portis, S. W. Ragsdale, T. B. Rauchfuss, J. N. H. Reek, L. C. Seefeldt, R. K. Thauer and G. L. Waldrop, Frontiers, Opportunities, and Challenges in Biochemical and Chemical Catalysis of CO_2 Fixation, *Chem. Rev.*, 2013, **113**, 6621–6658; (*d*) W.-H. Wang, Y. Himeda, J. T. Muckerman, G. F. Manbeck and E. Fujita, CO_2 Hydrogenation to Formate and Methanol as an Alternative to Photo- and Electrochemical CO_2 Reduction, *Chem. Rev.*, 2015, **115**, 12936–12973; (*e*) M. Limbach, 'Chapter Four - Acrylates from Alkenes and CO_2, the Stuff That Dreams Are Made of'. in *Advances in Organometallic Chemistry*, ed. Pérez P. J., Academic Press, 2015, pp. 175–202; (*f*) W. H. Bernskoetter and N. Hazari, Reversible Hydrogenation of Carbon Dioxide to Formic Acid and Methanol: Lewis Acid Enhancement of Base Metal Catalysts, *Acc. Chem. Res.*, 2017, **50**, 1049–1058; (*g*) J. Artz, T. E. Müller, K. Thenert, J. Kleinekorte, R. Meys, A. Sternberg, A. Bardow and W. Leitner, Sustainable Conversion of Carbon Dioxide: An Integrated Review of Catalysis and Life Cycle Assessment, *Chem. Rev.*, 2018, **118**, 434–504; (*h*) M. D. Burkart, N. Hazari, C. L. Tway and E. L. Zeitler, Opportunities and Challenges for Catalysis in Carbon Dioxide Utilization, *ACS Catal.*, 2019, **9**, 7937–7956; (*i*) C. Hepburn, E. Adlen, J. Beddington, E. A. Carter, S. Fuss, N. Mac Dowell, J. C. Minx, P. Smith and C. K. Williams, The Technological and Economic Prospects for CO_2 Utilization and Removal, *Nature*, 2019, **575**, 87–97; (*j*) Z. Zhang, S.-Y. Pan, H. Li, J. Cai, A. G. Olabi, E. J. Anthony and V. Manovic, Recent Advances in Carbon Dioxide Utilization, *Renewable Sustainable Energy Rev.*, 2020, **125**, 109799; (*k*) W. Gao, S. Liang, R. Wang, Q. Jiang, Y. Zhang, Q. Zheng, B. Xie, C. Y. Toe, X. Zhu, J. Wang, L. Huang, Y. Gao, Z. Wang, C. Jo, Q. Wang, L. Wang, Y. Liu, B. Louis, J. Scott, A.-C. Roger, R. Amal, H. He and S.-E. Park, Industrial Carbon Dioxide Capture and Utilization: State of the Art and Future Challenges, *Chem. Soc. Rev.*, 2020, **49**, 8584–8686.

2 National Academies of Sciences, Engineering, and Medicine, *Gaseous Carbon Waste Streams Utilization: Status and Research Needs*, The National Academies Press, Washington DC, 2019.

3 (*a*) K. Huang, C.-L. Sun and Z.-J. Shi, Transition-Metal Catalyzed C-C Bond Formation Through the Fixation of Carbon Dioxide, *Chem. Soc. Rev.*, 2011, **40**, 2435–2452; (*b*) I. Omae, Recent Developments in Carbon Dioxide Utilization for the Production of Organic Chemicals, *Coord. Chem. Rev.*, 2012, **256**, 1384–1405; (*c*) Y. Tsuji and T. Fujihara, Carbon Dioxide as a Carbon Source in Organic Transformation: Carbon-Carbon Bond Forming Reactions

by Transition-Metal Catalysts, *Chem. Commun.*, 2012, **48**, 9956–9964; (*d*) C. S. Yeung and V. M. Dong, Making C-C Bonds from Carbon Dioxide *via* Transition-Metal Catalysis, *Top. Catal.*, 2014, **57**, 1342–1350; (*e*) Q. Liu, L. Wu, R. Jackstell and M. Beller, Using Carbon Dioxide as a Building Block in Organic Synthesis, *Nat. Commun.*, 2015, **6**, 5933; (*f*) D. Yu, S. P. Teong and Y. Zhang, Transition Metal Complex Catalyzed Carboxylation Reactions with CO_2, *Coord. Chem. Rev.*, 2015, **293–294**, 279–291; (*g*) A.-H. Liu, B. Yu and L.-N. He, Catalytic Conversion of Carbon Dioxide to Carboxylic Acid Derivatives, *Greenhouse Gases: Sci. Technol.*, 2015, **5**, 17–33; (*h*) M. Börjesson, T. Moragas, D. Gallego and R. Martin, Metal-Catalyzed Carboxylation of Organic (Pseudo)halides with CO_2, *ACS Catal.*, 2016, **6**, 6739–6749; (*i*) A. Tortajada, F. Juliá-Hernández, M. Börjesson, T. Moragas and R. Martin, Transition-Metal-Catalyzed Carboxylation Reactions with Carbon Dioxide, *Angew. Chem., Int. Ed.*, 2018, **57**, 15948–15982; (*j*) M. Obst, L. Pavlovic and K. H. Hopmann, Carbon-Carbon Bonds with CO_2: Insights from Computational Studies, *J. Organomet. Chem.*, 2018, **864**, 115–127; (*k*) Y. Yang and J.-W. Lee, Toward Ideal Carbon Dioxide Functionalization, *Chem. Sci.*, 2019, **10**, 3905–3926; (*l*) J. Hong, M. Li, J. Zhang, B. Sun and F. Mo, C−H Bond Carboxylation with Carbon Dioxide, *ChemSusChem*, 2019, **12**, 6–39; (*m*) C. S. Yeung, Photoredox Catalysis as a Strategy for CO_2 Incorporation: Direct Access to Carboxylic Acids from a Renewable Feedstock, *Angew. Chem., Int. Ed.*, 2019, **58**, 5492–5502.

4 N. Hazari and J. E. Heimann, Carbon Dioxide Insertion into Group 9 and 10 Metal-Element σ-Bonds, *Inorg. Chem.*, 2017, **56**, 13655–13678.

5 (*a*) J. E. Heimann, W. H. Bernskoetter, N. Hazari and J. M. Mayer, Acceleration of CO_2 Insertion into Metal Hydrides: Ligand, Lewis Acid, and Solvent Effects on Reaction Kinetics, *Chem. Sci.*, 2018, **8**, 6629–6638; (*b*) J. E. Heimann, W. H. Bernskoetter and N. Hazari, Understanding the Individual and Combined Effects of Solvent and Lewis Acid on CO_2 Insertion into a Metal Hydride, *J. Am. Chem. Soc.*, 2019, **141**, 10520–10529.

6 For an example of CO_2 insertion into a Sc alkyl bond see: F. A. LeBlanc, A. Berkefeld, W. E. Piers and M. Parvez, Reactivity of Scandium β-Diketiminate Alkyl Complexes with Carbon Dioxide, *Organometallics*, 2012, **31**, 810–818.

7 For an example of CO_2 insertion into a Zr alkyl bond see: K.-C. Lau, B. J. Petro, S. Bontemps and R. F. Jordan, Comparative Reactivity of Zr–and Pd–Alkyl Complexes with Carbon Dioxide, *Organometallics*, 2013, **32**, 6895–6898.

8 For an example of CO_2 insertion into a Cr alkyl bond see: D. J. Darensbourg and A. Rokicki, Reduction of Carbon Dioxide and Carbonyl Sulfide by Anionic Group VIB Metal Hydrides and Alkyls. Carbon-Hydrogen and Carbon-Carbon Bond Formation Processes and the Structure of [PNP][$Cr(CO)_5SC(O)H$], *J. Am. Chem. Soc.*, 1982, **104**, 349–350.

9 For examples of CO_2 insertion into W-alkyl bonds see: (*a*) D. J. Darensbourg, R. K. Hanckel, C. G. Bauch, M. Pala, D. Simmons and J. N. White, A Kinetic Investigation of Carbon Dioxide Insertion Processes Involving Anionic Tungsten-Alkyl and -Aryl Derivatives: Effects of Carbon Dioxide Pressure, Counterions, and Ancillary Ligands. Comparisons with Migratory Carbon Monoxide Insertion Processes, *J. Am. Chem. Soc.*, 1985, **107**, 7463–7473; (*b*) D. J. Darensbourg and M. Pala, Cation-Anion Interaction in the [Na-kryptofix-221][$W(CO)_5O_2CH$] Derivative and its Relevance in Carbon Dioxide Reduction Processes, *J. Am. Chem. Soc.*, 1985, **107**, 5687–5693; (*c*) D. J. Darensbourg and G. Grotsch, Stereochemical Studies of the Carbon Dioxide Insertion Reactions into the Tungsten-Alkyl Bond, *J. Am. Chem. Soc.*, 1985, **107**, 7473–7476; (*d*) D. J. Darensbourg and R. Kudaroski, Metal-Induced Transformations of Carbon Dioxide. Carbon-Carbon Bond-Forming Processes Involving Anionic Group VIB Metal Derivatives, and the X-ray structure of [PNP][cis-$MeW(CO)_4PMe_3$], *J. Am. Chem. Soc.*, 1984, **106**, 3672–3673.

10 For examples of CO_2 insertion into Fe-alkyl bonds see: (*a*) S. Ittel, C. Tolman, A. English and J. Jesson, The Chemistry of 2-Naphthyl bis[bis(dimethylphosphino)ethane] Hydride Complexes of Iron, Ruthenium, and Osmium. 2. Cleavage of sp and sp^3 Carbon-Hydrogen, Carbon-Oxygen, and Carbon-Halogen bonds. Coupling of Carbon Dioxide and Acetonitrile, *J. Am. Chem. Soc.*, 1978, **100**, 7577–7585; (*b*) I. M. Arafa, K. Shin and H. M. Goff, Carbon Monoxide and Carbon Dioxide Carbon-Metal Bond Insertion Chemistry of Alkyliron(III) Porphyrin Complexes, *J. Am. Chem. Soc.*, 1988, **110**, 5228–5229; (*c*) O. R. Allen, S. J. Dalgarno, L. D. Field, P. Jensen, A. J. Turnbull and A. C. Willis, Addition of CO_2 to Alkyl Iron complexes, $Fe(PP)_2Me_2$, *Organometallics*, 2008, **27**, 2092–2098; (*d*) K.-C. Lau and R. F. Jordan, Reactivity of (Pyridine-Diimine) Fe Alkyl Complexes with Carbon Dioxide, *Organometallics*, 2016, **35**, 3658–3666.

11 For examples of CO_2 insertion into Ru-alkyl bonds see reference 10a and: (*a*) O. R. Allen, S. J. Dalgarno, L. D. Field, P. Jensen and A. C. Willis, Insertion of CO_2 into the Ru−C Bonds of cis-and trans-$Ru(dmpe)_2Me_2$ (dmpe = $Me_2PCH_2CH_2PMe_2$), *Organometallics*, 2009, **28**, 2385–2390; (*b*) J. F. Hartwig, R. G. Bergman and R. A. Andersen, Insertion Reactions of Carbon Monoxide and Carbon Dioxide with Ruthenium Benzyl, Arylamido, and Aryloxide complexes: A Comparison of the Reactivity of Ruthenium-Carbon, Ruthenium-Nitrogen, and Ruthenium-Oxygen Bonds, *J. Am. Chem. Soc.*, 1991, **113**, 6499–6508.

12 For examples of CO_2 insertion into Rh-alkyl bonds see: (*a*) D. J. Darensbourg, G. Groetsch, P. Wiegreffe and A. L. Rheingold, Insertion Reactions of Carbon Dioxide with Square-Planar Rhodium Alkyl and Aryl Complexes, *Inorg. Chem.*, 1987, **26**, 3827–3830; (*b*) T. G. Ostapowicz, M. Hölscher and W. Leitner, CO_2 Insertion into Metal–Carbon Bonds: A Computational Study of RhI Pincer Complexes, *Chem. – Eur. J.*, 2011, **17**, 10329–10338; (*c*) T. Suga, T. Saitou, J. Takaya and N. Iwasawa, Mechanistic Study of the Rhodium-Catalyzed Carboxylation of Simple Aromatic Compounds with Carbon Dioxide, *Chem. Sci.*,

2017, **8**, 1454–1462; (*d*) L. Pavlovic, J. Vaitla, A. Bayer and K. H. Hopmann, Rhodium-Catalyzed Hydrocarboxylation: Mechanistic Analysis Reveals Unusual Transition State for Carbon–Carbon Bond Formation, *Organometallics*, 2018, **37**, 941–948.

13 For examples of CO_2 insertion into Cu-alkyl bonds see: (*a*) T. Ikariya and A. Yamamoto, Preparation and Properties of Ligand-Free Methylcopper and of Copper Alkyls Coordinated with 2,2′-Bipyridyl and Tricyclohexylphosphine, *J. Organomet. Chem.*, 1974, **72**, 145–151; (*b*) N. P. Mankad, T. G. Gray, D. S. Laitar and J. P. Sadighi, Synthesis, Structure, and CO_2 Reactivity of a Two-Coordinate (Carbene)copper(I) Methyl Complex, *Organometallics*, 2004, **23**, 1191–1193; (*c*) S. Sakaki and K. Ohkubo, Ab initio MO Study of Carbon Dioxide Insertion into a Methyl-Copper(I) Bond. Critical Difference from CO_2 Insertion into a Hydrogen-Copper(I) Bond, *Organometallics*, 1989, **8**, 2970–2973.

14 The following examples describe CO_2 insertion into Ni(I) alkyl species. In both cases, the starting materials and products are highly unstable, which precludes detailed kinetic studies. (*a*) J. B. Diccianni, C. T. Hu and T. Diao, Insertion of CO_2 Mediated by a (Xantphos)NiI–Alkyl Species, *Angew. Chem., Int. Ed.*, 2019, **58**, 13865–13868; (*b*) R. J. Somerville, C. Odena, M. F. Obst, N. Hazari, K. H. Hopmann and R. Martin, Ni(I)–Alkyl Complexes Bearing Phenanthroline Ligands: Experimental Evidence for CO_2 Insertion at Ni(I) Centers, *J. Am. Chem. Soc.*, 2020, **142**, 10936–10941.

15 R. Johansson, M. Jarenmark and O. F. Wendt, Insertion of Carbon Dioxide into (PCP)Pd^{II}-Me Bonds, *Organometallics*, 2005, **24**, 4500–4502.

16 T. J. Schmeier, N. Hazari, C. D. Incarvito and J. R. Raskatov, Exploring the Reactions of CO_2 with PCP Supported Nickel Complexes, *Chem. Commun.*, 2011, **47**, 1824–1826.

17 (*a*) K. J. Jonasson and O. F. Wendt, Synthesis and Characterization of a Family of POCOP Pincer Complexes with Nickel: Reactivity Towards CO_2 and Phenylacetylene, *Chem. – Eur. J.*, 2014, **20**, 11894–11902; (*b*) A. H. Mousa, J. Bendix and O. F. Wendt, Synthesis, Characterization, and Reactivity of PCN Pincer Nickel Complexes, *Organometallics*, 2018, **37**, 2581–2593; (*c*) A. H. Mousa, A. V. Polukeev, J. Hansson and O. F. Wendt, Carboxylation of the Ni–Me Bond in an Electron-Rich Unsymmetrical PCN Pincer Nickel Complex, *Organometallics*, 2020, **39**, 1553–1560.

18 (*a*) C. Reichardt, Empirical Parameters of the Polarity of Solvents, *Angew. Chem., Int. Ed.*, 1965, **4**, 29–40; (*b*) C. Reichardt, Solvatochromic Dyes as Solvent Polarity Indicators, *Chem. Rev.*, 1994, **94**, 2319–2358.

19 H.-W. Suh, T. J. Schmeier, N. Hazari, R. A. Kemp and M. K. Takase, Experimental and Computational Studies of the Reaction of Carbon Dioxide with Pincer-Supported Nickel and Palladium Hydrides, *Organometallics*, 2012, **31**, 8225–8236.

20 S. J. Mitton, R. McDonald and L. Turculet, Nickel and Palladium Silyl Pincer Complexes: Unusual Structural Rearrangements that Involve Reversible Si-C(sp^3) and Si-C(sp^2) Bond Activation, *Angew. Chem., Int. Ed.*, 2009, **48**, 8568–8571.

21 (*a*) Y. Segawa, M. Yamashita and K. Nozaki, Syntheses of PBP Pincer Iridium Complexes: A Supporting Boryl Ligand, *J. Am. Chem. Soc.*, 2009, **131**, 9201–9203; (*b*) Y. Segawa, M. Yamashita and K. Nozaki, Diphenylphosphino- or Dicyclohexylphosphino-Tethered Boryl Pincer Ligands: Syntheses of PBP Iridium(III) Complexes and Their Conversion to Iridium−Ethylene Complexes, *Organometallics*, 2009, **28**, 6234–6242; (*c*) A. F. Hill, S. B. Lee, J. Park, R. Shang and A. C. Willis, Analogies between Metallaboratranes, Triboronates, and Boron Pincer Ligand Complexes, *Organometallics*, 2010, **29**, 5661–5669; (*d*) M. Hasegawa, Y. Segawa, M. Yamashita and K. Nozaki, Isolation of a PBP-Pincer Rhodium Complex Stabilized by an Intermolecular C-H σCoordinationas the Fourth Ligand, *Angew. Chem., Int. Ed.*, 2012, **51**, 6956–6960; (*e*) H. Ogawa and M. Yamashita, Platinum Complexes Bearing a Boron-Based PBP Pincer Ligand: Synthesis, Structure, and Application as a Catalyst for Hydrosilylation of 1-Decene, *Dalton Trans.*, 2013, **42**, 625–629; (*f*) T. Miyada and M. Yamashita, Oxygenation of a Ruthenium Complex Bearing a PBP-Pincer Ligand Inducing the Formation of a Boronato Ligand with a Weak Ru–O Bond, *Organometallics*, 2013, **32**, 5281–5284; (*g*) T.-P. Lin and J. C. Peters, Boryl–Metal Bonds Facilitate Cobalt/Nickel-Catalyzed Olefin Hydrogenation, *J. Am. Chem. Soc.*, 2014, **136**, 13672–13683; (*h*) N. Curado, C. Maya, J. López-Serrano and A. Rodríguez, Boryl-Assisted Hydrogenolysis of a Nickel–Methyl Bond, *Chem. Commun.*, 2014, **50**, 15718–15721; (*i*) P. Ríos, N. Curado, J. López-Serrano and A. Rodríguez, Selective Reduction of Carbon Dioxide to Bis(silyl)acetal Catalyzed by a PBP-Supported Nickel Complex, *Chem. Commun.*, 2016, **52**, 2114–2117; (*j*) P. Rios, A. Rodriguez and J. Lopez-Serrano, Mechanistic Studies on the Selective Reduction of CO_2 to the Aldehyde Level by a Bis(phosphino)boryl (PBP)-Supported Nickel Complex, *ACS Catal.*, 2016, **6**, 5715–5723; (*k*) Y. Ding, Q.-Q. Ma, J. Kang, J. Zhang, S. Li and X. Chen, Palladium(II) Complexes Supported by PBP and POCOP Pincer Ligands: A Comparison of their Structure, Properties and Catalytic Activity, *Dalton Trans.*, 2019, **48**, 17633–17643.

22 D. Adhikari, J. C. Huffman and D. J. Mindiola, Structural Elucidation of a Nickel Boryl Complex. A Recyclable Borylation Ni(II) Reagent of Bromobenzene, *Chem. Commun.*, 2007, 4489–4491.

23 (*a*) H. Clavier and S. P. Nolan, Percent Buried Volume for Phosphine and N-Heterocyclic Carbene Ligands: Steric Properties in Organometallic Chemistry, *Chem. Commun.*, 2010, **46**, 841–861; (*b*) L. Falivene, R. Credendino, A. Poater, A. Petta, L. Serra, R. Oliva, V. Scarano and L. Cavallo, SambVca 2. A Web Tool for Analyzing Catalytic Pockets with Topographic Steric Maps, *Organometallics*, 2016, **35**, 2286–2293.

24 B. F. M. Kimmich, W. J. Marshall, P. J. Fagan, E. Hauptman and R. M. Bullock, Palladium Complexes with PCP Ligands:

Preparation and Structural Studies of Two Forms of [(PCP)Pd(OH_2)]$^+BF4^-$, *Inorg. Chim. Acta*, 2002, **330**, 52–58.

25 (*a*) R. Beck, M. Shoshani, J. Krasinkiewicz, J. A. Hatnean and S. A. Johnson, Synthesis and Chemistry of Bis(triisopropylphosphine) Nickel(I) and Nickel(0) Precursors, *Dalton Trans.*, 2013, **42**, 1461–1475; (*b*) W. H. Harman, T.-P. Lin and J. C. A. Peters, d^{10} Ni–(H_2) Adduct as an Intermediate in H-H Oxidative Addition across a Ni-B Bond, *Angew. Chem., Int. Ed.*, 2014, **53**, 1081–1086; (*c*) Y.-E. Kim, J. Kim and Y. Lee, Formation of a Nickel Carbon Dioxide Adduct and its Transformation Mediated by a Lewis Acid, *Chem. Commun.*, 2014, **50**, 11458–11461; (*d*) Y.-E. Kim, S. Oh, S. Kim, O. Kim, J. Kim, S. W. Han and Y. Lee, Phosphinite-Ni(0) Mediated Formation of a Phosphide-Ni(II)-OCOOMe Species *via* Uncommon Metal–Ligand Cooperation, *J. Am. Chem. Soc.*, 2015, **137**, 4280–4283; (*e*) D. J. Charboneau, D. Balcells, N. Hazari, H. M. C. Lant, J. M. Mayer, P. R. Melvin, B. Q. Mercado, W. D. Morris, M. Repisky and H.-W. Suh, Dinitrogen-Facilitated Reversible Formation of a Si–H Bond in a Pincer-Supported Ni Complex, *Organometallics*, 2016, **35**, 3154–3162.

26 M. T. Johnson, R. Johansson, M. V. Kondrashov, G. Steyl, M. S. G. Ahlquist, A. Roodt and O. F. Wendt, Mechanisms of the CO_2 Insertion into (PCP) Palladium Allyl and Methyl σ-Bonds. A Kinetic and Computational Study, *Organometallics*, 2010, **29**, 3521–3529.

27 U. Mayer, V. Gutmann and W. Gerger, The Acceptor Number — A Quantitative Empirical Parameter for the Electrophilic Properties of Solvents, *Monatsh. Chem.*, 1975, **106**, 1235–1257.

28 D. J. Charboneau, G. W. Brudvig, N. Hazari, H. M. Lant and A. K. Saydjari, Development of an Improved System for the Carboxylation of Aryl Halides Through Mechanistic Studies, *ACS Catal.*, 2019, **9**, 3228–3241.

29 THF was selected as the solvent due to the improved solubility of many Lewis acids in THF compared to other ethereal solvents.

30 D. García-López, L. Pavlovic and K. H. Hopmann, To Bind or Not to Bind: Mechanistic Insights into C–CO_2 Bond Formation with Late Transition Metals, *Organometallics*, 2020, **39**, 1339–1347.

31 We also calculated CO_2 insertion into (^{Me}PCP)Pd(CH_3), where the *tert*-butyl substituents on the ^{tBu}PCP ligand have been replaced with methyl substituents. The calculations indicate that for (^{Me}PCP)Pd(CH_3), the 1,2-insertion pathway is preferred over the S_E2 mechanism by 1.8 kcal mol^{-1} (Table 3, Fig. S53 and S54†). This is consistent with the hypothesis that the steric properties of the pincer ligand play a large role in determining the pathway for CO_2 insertion.

32 We note that other computational protocols (ωB97XD, PBE0-D3BJ) provide the same reactivity trends as B3LYP-D3 (Table S3†).

33 Our results do not explain Wendt's observation (see ref. 17b and 17c) that CO_2 insertion into (^{t}Bu^{i}PrN)Ni(CH_3) (^{t}Bu^{i}PrN = 1-(3-((ditert-butylphosphino)methyl)phenyl)-*N*,*N*-diisopropyl-methanamine)) is faster than insertion into (^{t}Bu^{Me}N)Ni(CH_3) (^{t}Bu^{Me}N = 1-(3-((ditert-butylphosphino)methyl)phenyl)-*N*,*N*-methyl-methanamine)). In this case, ligand hemilability may play a role and it is possible that the more sterically bulky ^{t}Bu^{i}PrN is more likely to decoordinate.